

Article

Two-Step Synthesis, Structure, and Optical Features of a Double Hetero[7]helicene

Mohamed S. H. Salem ^{1,2} , Ahmed Sabri ¹ , Md. Imrul Khalid ¹ , Hiroaki Sasai ^{1,3}  and Shinobu Takizawa ^{1,*}¹ SANKEN, Osaka University, Ibaraki-shi, Osaka 567-0047, Japan² Pharmaceutical Organic Chemistry Department, Faculty of Pharmacy, Suez Canal University, Ismailia 41522, Egypt³ Graduate School of Pharmaceutical Sciences, Osaka University, Suita-shi, Osaka 565-0871, Japan

* Correspondence: taki@sanken.osaka-u.ac.jp; Tel.: +81-6-6879-8467

Abstract: A novel double aza-oxa[7]helicene was synthesized from the commercially available N^1, N^4 -di(naphthalen-2-yl)benzene-1,4-diamine and *p*-benzoquinone in two steps. Combining the acid-mediated annulation with the electrochemical sequential reaction (oxidative coupling and dehydrative cyclization) afforded this double hetero[7]helicene. Moreover, the structural and optical features of this molecule have been studied using X-ray crystallographic analysis, and the absorption and emission behaviors were rationalized based on DFT calculations.

Keywords: polycyclic aromatic hydrocarbon; double hetero[7]helicene; short-step synthesis; electrochemical cross-coupling; nucleus-independent chemical shift



Citation: Salem, M.S.H.; Sabri, A.; Khalid, M.I.; Sasai, H.; Takizawa, S. Two-Step Synthesis, Structure, and Optical Features of a Double Hetero[7]helicene. *Molecules* **2022**, *27*, 9068. <https://doi.org/10.3390/molecules27249068>

Academic Editor: Mircea Darabantu

Received: 29 November 2022

Accepted: 14 December 2022

Published: 19 December 2022

Publisher's Note: MDPI stays neutral with regard to jurisdictional claims in published maps and institutional affiliations.



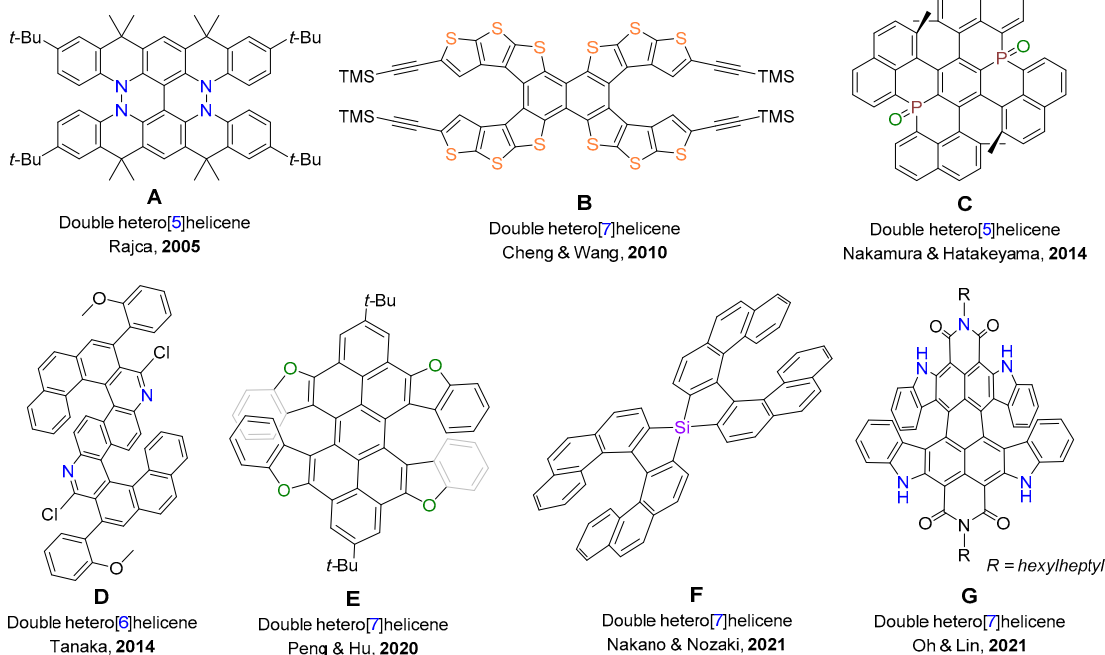
Copyright: © 2022 by the authors. Licensee MDPI, Basel, Switzerland. This article is an open access article distributed under the terms and conditions of the Creative Commons Attribution (CC BY) license (<https://creativecommons.org/licenses/by/4.0/>).

1. Introduction

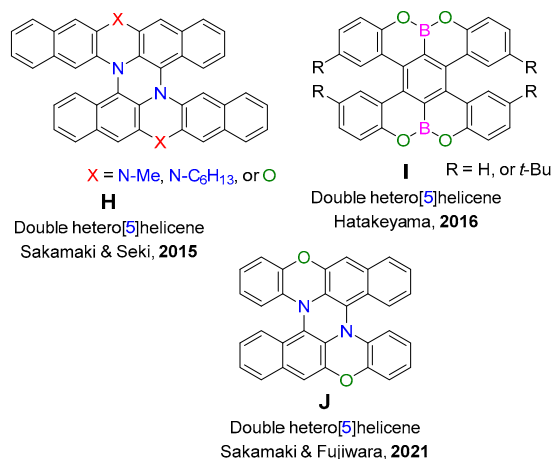
Helicenes are polycyclic aromatic hydrocarbons (PAHs) in which aromatic rings are annulated in a helical architecture, giving them unique electronic, photophysical and chiroptical properties [1–4]. Over the past couple of decades, the great advances achieved in this chemistry [2–6] promoted a broad spectrum of material-based applications [7–10], transistors [11,12], and semiconductors [13]. Incorporation of one or more heteroatoms in the helicene scaffolds modulate their physical and optical features, and alter the electronic properties in order to expand their applications [14,15]. With these extra features, the trend in helicene chemistry has begun to move towards heterohelicenes after the domination of carbohelicenes [16–21]. Another approach to promote characteristics of helicenes is to induce multihelicity which means combining two or more helical scaffolds in a single molecule [22,23]. Multiple helicenes show a lot of favorable properties due to their amplified non-planarity, diverse conformations, and maximized intermolecular interactions [24,25]. Various smart core scaffolds were used to induce this multihelicity such as perylene diimide (PDI) that afforded valuable twisted structures for different material-based applications [26–29]. Hence, a lot of efforts were dedicated for designing and synthesizing multiple heterohelicenes [30], in particular, double heterohelicenes [14]. After the first report of double helicene reported by Rajca, many examples of these double heterohelicenes were conducted and exhibited clear superiority over their single counterparts, especially in terms of optical properties (Figure 1a) [31–40]. However, during that frantic pursuit to promote the properties of helicenes, another problem, in particular, synthetic difficulty emerged. With the increase in structural complexity, the synthesis of multiple heterohelicenes becomes more challenging and requires many steps. Although few reports succeeded to introduce effective short-step synthetic protocols for double heterohelicene, most of these successes were concentrated in the double hetero[5]helicene derivatives (Figure 1b) [41–43]. In 2016, Narita, Cao, and Müllen introduced an efficient two-step synthesis of a highly strained OBO-fused double hetero[7]helicene **K** via the nucleophilic aromatic substitution reaction of hexabromobenzene, followed by a sequential

step of demethylation and C-H aryl borylation (Figure 1c) [44]. Earlier in the same year, Hatakeyama showed the potential of this synthetic approach to afford their boron-fused double hetero[5]helicene **I** (Figure 1b) [42]. In 2021, Wang and coworkers developed the first examples of B,N-embedded double hetero[7]helicenes **L** that showed excellent chiroptical features in the visible range [45]. With only two steps, they succeeded to prepare this double hetero[7]helicene **L** via the nucleophilic aromatic substitution of dibromotetrafluorobenzene with carbazole, followed by a tandem process of substitution with BBr_3 and C-H aryl borylation [45].

(a) Selected examples of double heterohelicenes



(b) Selected examples of double hetero[5]helicenes (that can be synthesized by short-steps '2-3 steps')



(c) Selected examples of double hetero[7]helicenes (that can be synthesized by two-steps)

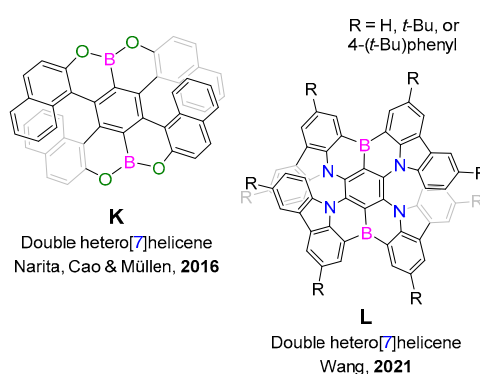


Figure 1. The selected examples of double heterohelicenes in short-step synthesis: (a) Double hetero[5–7]helicenes (more than four-step synthesis); (b) Double hetero[5]helicenes (two- or three-step synthesis); (c) Double hetero[7]helicenes (two-step synthesis).

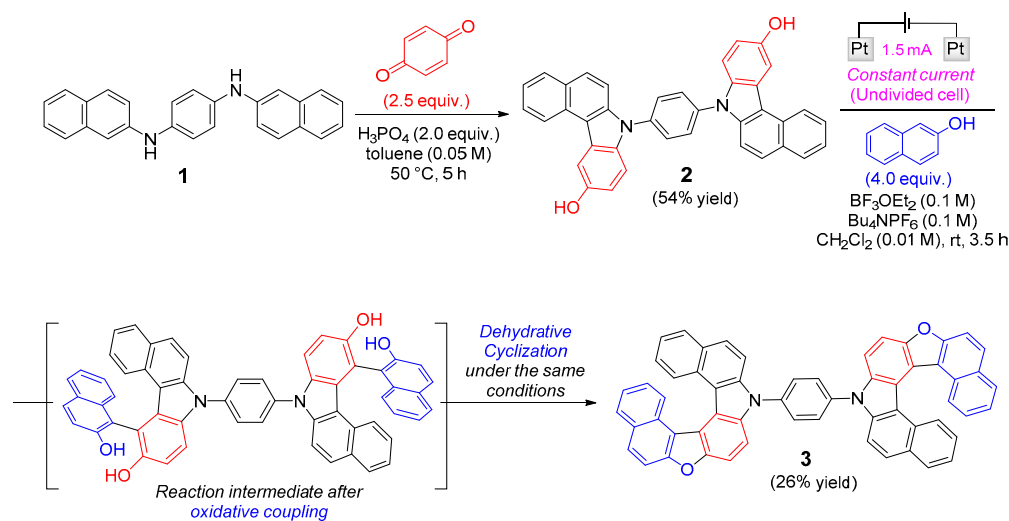
Notably, these examples (Figure 1c) represent a quantum leap in the short-step synthesis of double hetero[7]helicenes via the tandem process of nucleophilic substitution with BBr_3 followed by C-H aryl borylation [44,45]. As part of our effort to explore the

electrochemical domino syntheses, we were interested in designing effective sequential reactions to access double helicene motifs [46,47]. Herein, a facile preparation of a double aza-oxa[7]helicene with a phenylene linker has been established through acid-mediated annulation with the electrochemical sequential reaction (oxidative coupling and dehydrative cyclization). We also studied the structural and optical features via x-ray crystallographic analysis, spectrophotometric analysis, and DFT calculations.

2. Results and Discussion

2.1. Synthesis of Double Aza-oxa[7]helicene 3

Recently, Zhang reported a facile acid-mediated synthesis of carbazole in which aniline derivatives react with *p*-benzoquinone to produce 3-hydroxycarbazoles [48]. Combining this approach with our unprecedented electrochemically enabled synthesis of hetero[7]helicenes and dehydro-hetero[7]helicenes [46,47], herein, we achieved the two-step synthesis of double aza-oxa[7]helicenes as depicted in Scheme 1. The acid-mediated annulation of the commercially available substrates; *N*¹,*N*⁴-di(naphthalen-2-yl)benzene-1,4-diamine **1** and *p*-benzoquinone afforded the corresponding bis-3-hydroxy-benzo[*c*]carbazole **2** in 54% yield via a tandem process of double Michael addition and subsequent double ring closure. Next, a DCM solution of **2**, β-naphthol, and tetrabutylammonium hexafluorophosphate(V) as an electrolyte, was utilized to a constant current of 1.5 mA in an undivided electrolysis cell with platinum electrodes for 3.5 h at room temperature, affording double aza-oxa[7]helicene **3** in 26% yield. The electrochemical sequential synthesis of **3** proceeds through the oxidative hetero-coupling of arenols to produce a diol intermediate that can readily undergo a subsequent dehydrative cyclization to **3**. All compounds showed good chemical and thermal stabilities and no decomposition was observed upon purification on silica column chromatography and heating at 100 °C in air.



Scheme 1. The synthesis of a double aza-oxa[7]helicenes **3**.

2.2. Structure and Packing Mode of 3

The double aza-oxa[7]helicene structure of **3** was definitely confirmed by X-ray crystallography using a single crystal, grown from its racemic solution. We used the liquid/liquid diffusion technique between ethyl acetate and *n*-hexane to prepare this crystal slowly over three days in a dark environment at −20 °C. As expected, the two helicene moieties are connected via a phenylene linker (Figure 2a,b). The dihedral angles between the phenylene linker's plane and the pyrrole (ring B') are −41.86° for (C₁-C₆-N₇-C₈), and 54.38° for (C₅-C₆-N₇-C₉). Although the experimental values of (C₅-C₆-N₇-C₉) dihedral angle (54.38°) is comparable to that of the optimized structure using DFT calculations at MN15/6-311G(d,p) level of theory (54.72°), (C₁-C₆-N₇-C₈) dihedral angle was smaller than optimized structures at various levels (Table 1). This can be attributed to the intermolecular

interactions between the double helicene molecules **3** in the packed structure. Only meso isomer (*P,M*)-**3** was observed in the crystal packing with achiral molecules packed along the *b*-axis (Figure 2c,d). The packing of **3** shows a herringbone pattern with π - π distance of 4.458 Å. This characteristic arrangement is optimum for many material-based applications, especially semiconductors [49–51]. In addition, it maximizes the optical and electronic properties of the obtained double helicene upon self-assembly [49,52–54]. Most of these larger or multiple helicenes showed significant variations during DFT calculations owing to the long-range conjugation and the effects of charge transfer [55,56]. Among the functions we screened, Minnesota 15 (MN15) function was found to be the most suitable parameters for our molecules (Table 1) [57].

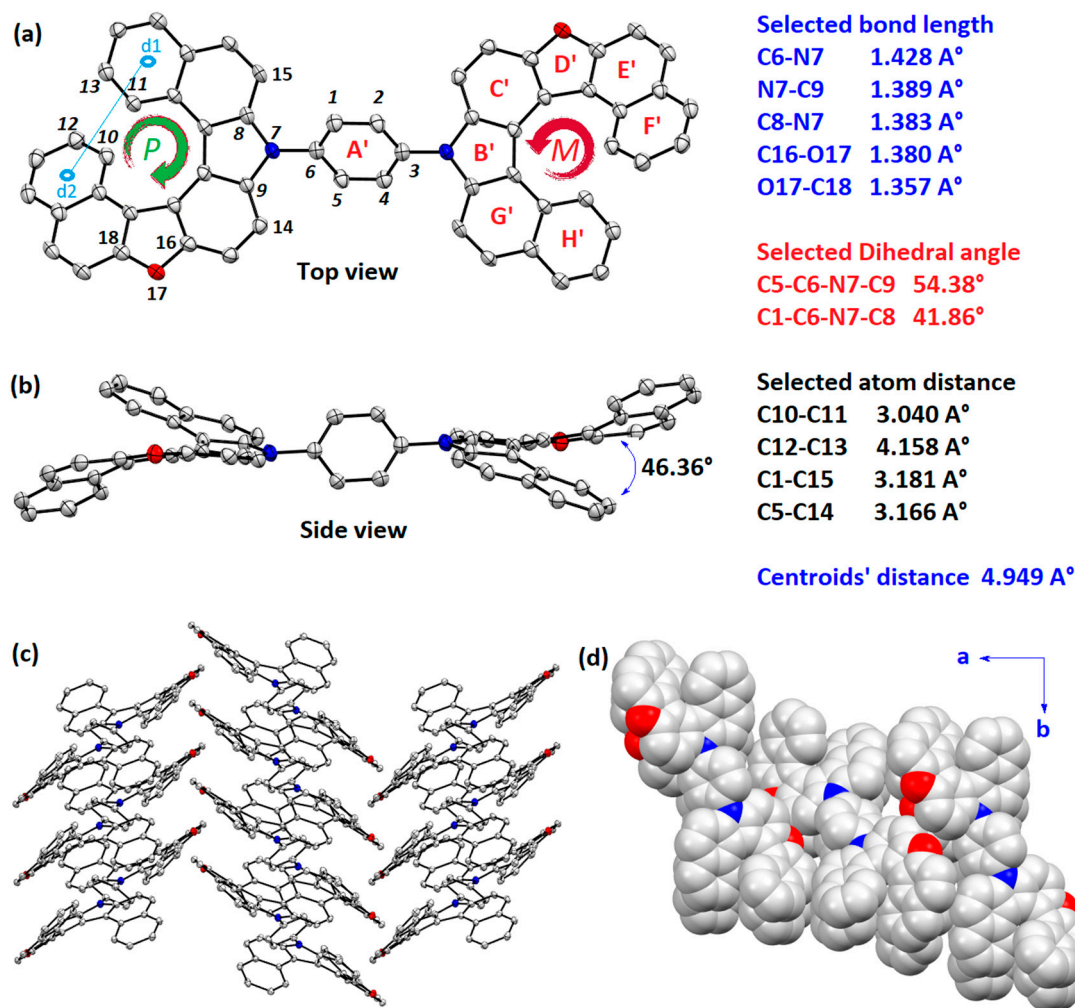


Figure 2. Single crystal structure of the double helicene **3**: (a,b) ORTEP drawing structure of (*P,M*)-**3** obtained by X-ray crystal analysis with ellipsoids at 50% probability (H atoms were omitted for clarity); (c) crystal packing of (*P,M*)-**3** with ellipsoids at 30% probability; (d) packing structure of (*P,M*)-**3** is viewed along the *c*-axis to show the herringbone arrangement.

Table 1. The selected experimental and calculated structural parameters of double aza-oxa[7]helicene **3**.

Parameters	Experimental	B3LYP ¹	wB97XD ¹	MN15 ¹
Centroids' distance (rings F'-H')	4.949 Å	4.885 Å	4.721 Å	4.759 Å
d ₁ -N ₇ -d ₂ Centroid angle	46.36°	45.43°	44.24°	45.51°
C ₅ -C ₆ -N ₇ -C ₉ Dihedral angle	54.38°	60.25°	59.03°	54.72°
C ₁ -C ₆ -N ₇ -C ₈ Dihedral angle	41.86°	57.08°	55.34°	51.42°
C ₁ -C ₁₅ Distance	3.181 Å	3.316 Å	3.281 Å	3.241 Å
C ₅ -C ₁₄ Distance	3.166 Å	3.356 Å	3.316 Å	3.266 Å

¹ All calculations are carried out using 6-311G(d,P) basis set at three different functions (B3LYP, wB97XD, and MN15).

Nucleus-independent chemical shift (NICS) calculations revealed the low aromaticity of the central phenylene linker with a NICS (0) value of -5.8 ppm (Figure 3a), much lower than that of benzene -7.6 ppm calculated at the same level of theory. The largest NICS (0) values (between -7.3 ppm and -8.6 ppm) were found on the benzene of 6*H*-furo[3,2-*e*]indole (ring C'), pyrrole (ring B') and naphthalene (rings F' and H'). While the lowest NICS (0) values (around -5.8 ppm) were found on the phenylene linker (ring A') and furan rings (D') which is consistent with the aromatic character of this ring. Generally, symmetric double hetero[*n*]helicenes ($n \geq 4$) have three isomers, those being two chiral enantiomers (*P,P*) and (*M,M*), and one meso diastereomer (*P,M*) [30]. All three isomers of **3** were afforded under our reaction conditions which was confirmed by HPLC separation using DAICEL CHIRALPAK IA column (eluent: *n*-hexane/*i*-PrOH = 20/1) (Figure 3b). The experimental ratio among the three isomers was found to be around (1:2:1) with the meso isomer (*P,M*)-**3** as the major formed product (confirmed by the absence of optical rotation). After HPLC chiral resolution, the epimerization rate of **3** was studied at three different temperatures (See SI). Eyring plot (Figure 3c) indicated a low chiral stability of **3** (epimerization barrier ~ 24.2 kcal mol⁻¹) with an estimated half-life of the epimerization <6.5 h at 25 °C. These observations were matching with our DFT calculations that showed similar epimerization barriers 25.32 kcal mol⁻¹ and 25.62 kcal mol⁻¹ (Figure 3d).

2.3. Photophysical Properties

Our double aza-oxa[7]helicene **3** shows high luminescence upon photo-irradiation, which can be attributed to the rigid scaffold that hinders the thermal energy loss upon structural changes. The UV/vis absorption of **3** was recorded in different solvents to show its high solubility in most of the organic solvents which increases the potential for some applications that require good solubility such as solution-processed electronics [58–60]. In all measured solvents, compound **3** showed similar UV/vis absorption patterns (Figure 4a). The maximum absorbance exhibited in chloroform was shown at 407 nm (absorption coefficient: 7.5×10^4 M⁻¹ cm⁻¹) corresponding to an optical energy gap of (2.18 eV). According to TD-DFT calculations at the MN15/6-311G(d,p) level of theory, this low-energy absorption can be accountable to the HOMO→LUMO transition. The absorption band at 385 nm possibly attributed to the equal contribution of both HOMO-1→LUMO and HOMO→LUMO+1 transitions. The band at 368 nm is estimated to be due to the HOMO-1→LUMO+1 transition, while the higher energy absorption band at 328 nm would be attributed to HOMO-2→LUMO corresponding to an optical energy gap of (2.58 eV). Molecular orbital calculations indicated that the HOMO is spread mainly over the phenylene linker (ring A') and pyrroles (rings B') and LUMO is spread over the whole scaffold rather than the phenylene linker (ring A'), accounting for the substantial stability. Photoluminescence PL spectrum of **3** was recorded in a pure chloroform solution exhibiting emission maxima shifted in a bathochromic way at 415 nm and 440 nm.

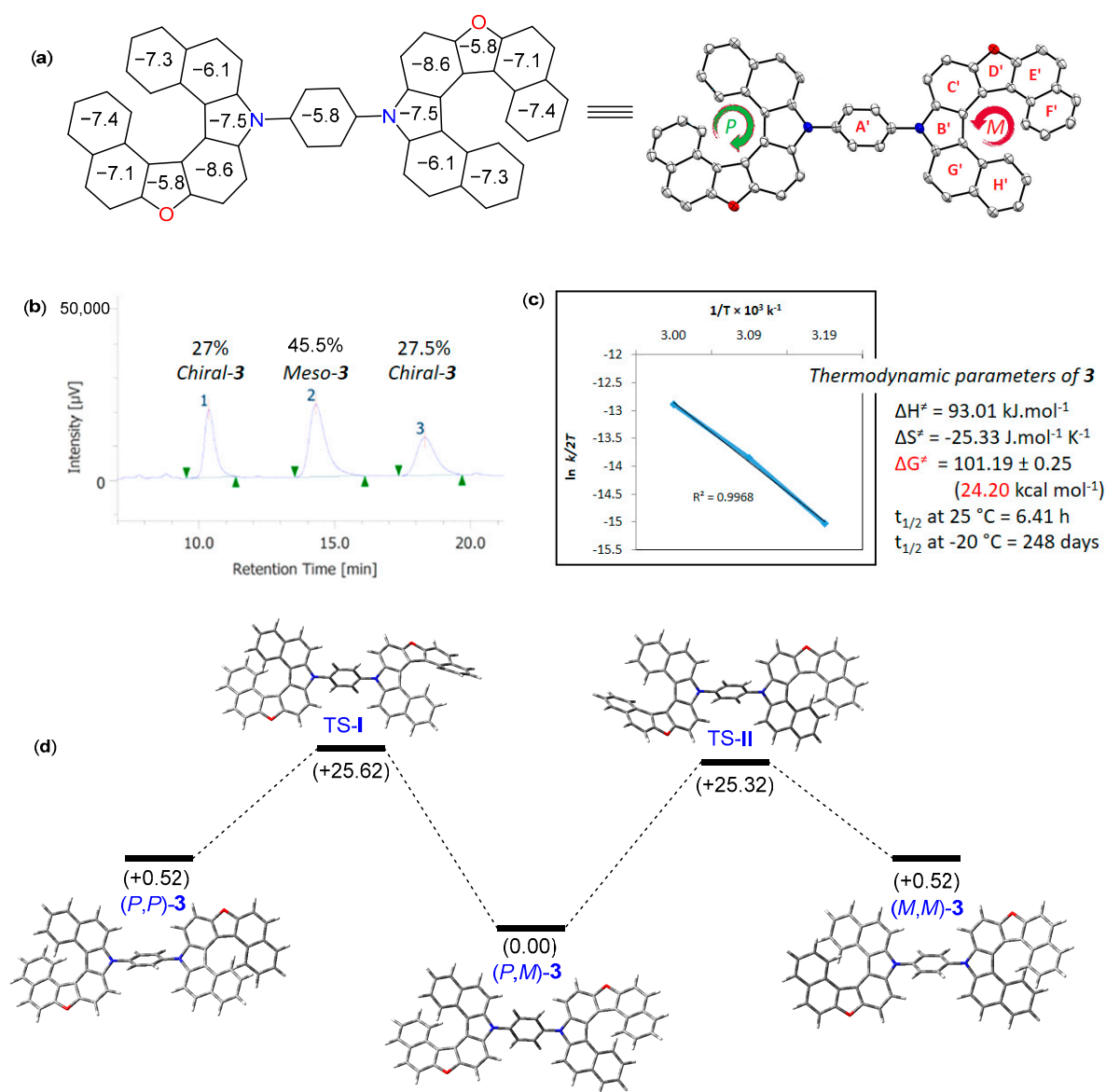


Figure 3. (a) NICS(0) values of (P,M) -3 calculated at the MN15/6-311G+(2d,p) level; (b) HPLC chromatogram determined by (Daicel Chiralpak IA, *n*-hexane/*i*-PrOH = 20/1, flow rate 1.0 mL/min, T = 25 °C, 240 nm): $t_1 = 10.36$ min, $t_2 = 14.30$ min, and $t_3 = 18.32$ min; (c) Eyring plot of compound 3 epimerization and thermodynamic parameters; (d) Epimerization process from (P,M) -3 isomer to (M,M) -3 and (P,P) -3 isomers. The relative Gibbs free energies are calculated in (kcal mol^{-1}) at the MN15/6-311G(d,p) level.

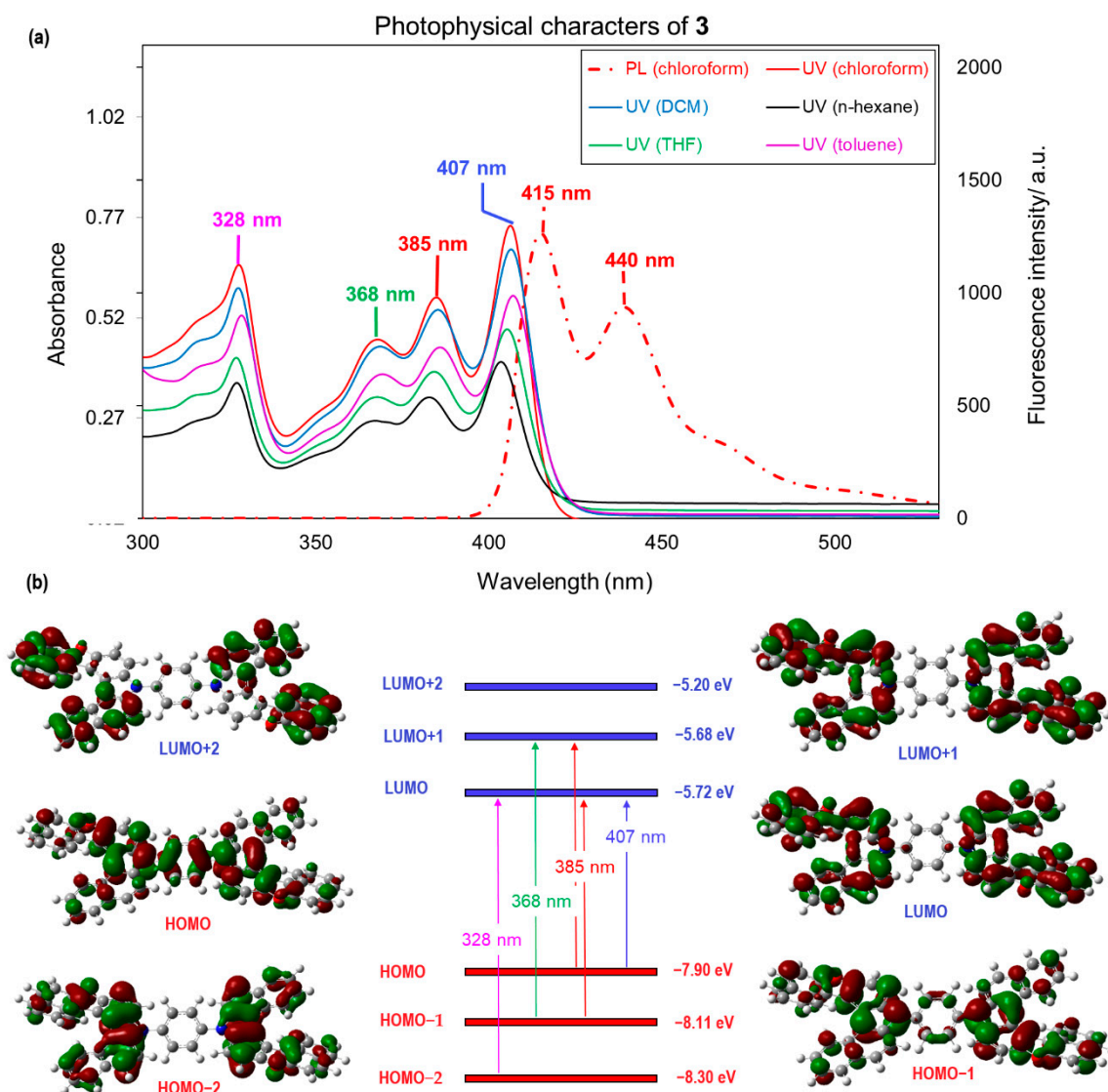


Figure 4. (a) UV/vis absorption and PL spectra of **3** in various solvents (20 μM); (b) Frontier Kohn-Sham molecular orbitals of **3** and TD-DFT calculated electronic transitions at MN15/6-311G (d,p) level of theory.

2.4. Energetic Characterization by Cyclic Voltammetry

Cyclic voltammetry (CV) measurements of our double aza-oxa[7]helicene **3** showed reversible redox peaks in both negative and positive regions indicating the chemical stability of its anion/cation pairs and how they can be reduced or oxidized readily to the neutral form (Figure 5). Using ferrocene and ferrocenium as internal references, the HOMO energy level of **3** was calculated using Bredas empirical equation to be around (−7.83 eV) which is comparable to the DFT-calculated HOMO energy (−7.90 eV) [61]. E_{LUMO} could be estimated after considering the gap between E_{HOMO} and E_{LUMO} (3.04 eV) from the λ_{max} or excitation energy (407 nm) to be around (−4.79 eV) showing little higher energy than the DFT-calculated LUMO (−5.72 eV).

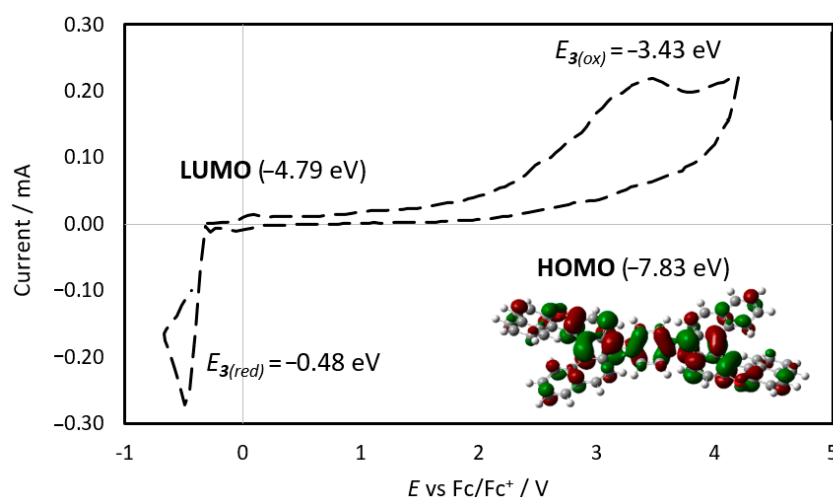


Figure 5. The cyclic voltammetry profile of **3** in (MeCN) with $n\text{-Bu}_4\text{NPF}_6$ (0.1 M) using ferrocene as internal reference.

3. Materials and Methods

3.1. General Experimental Details

^1H -, and ^{13}C -NMR were recorded via JNM ECA600 FT NMR (^1H -NMR 600 MHz, ^{13}C -NMR 151 MHz). ^1H -NMR spectra are reported as follows: a chemical shift in ppm downfield of tetramethylsilane (TMS) and referenced to residual solvent peak (CDCl_3) at 7.26 ppm, or ($(\text{CD}_3)_2\text{CO}$) at 2.05 ppm, multiplicities (s = singlet, d = doublet, dd = doublet of doublets, t = triplet, q = quartet, m = multiplet), and coupling constants (Hz). ^{13}C -NMR spectra reported in ppm relative to the central line of triplet for CDCl_3 at 77.16 ppm, or the central line of septet for $(\text{CD}_3)_2\text{CO}$ at 29.84 ppm. APCI-MS spectra were obtained with JMS-T100LC (JEOL). FT-IR spectra were recorded on a JASCO FT-IR system (FT/IR4100). Photoluminescence (PL) spectra were recorded on JASCO FP-8550 Spectrofluorometer. UV spectra were recorded on a JASCO v-770 spectrophotometer. Column chromatography on SiO_2 was performed with Kanto Silica Gel 60 (63–210 μm). Commercially available organic and inorganic compounds were used without further purification. The electro-oxidation was carried out using sing ElectraSyn[®] 2.0 (designed by IKA) at a constant current of 1.5 mA, under air (1 atm.) [62].

3.2. Synthetic Procedures

3.2.1. General Procedure for the Synthesis of Double 3-Hydroxy Benzo[c]carbazole **2**

To a solution of N^1, N^4 -di(naphthalen-2-yl)benzene-1,4-diamine **1** (36 mg, 0.1 mmol) and *p*-benzoquinone (27 mg, 0.25 mmol, 2.5 equiv.) in dry toluene (1.5 mL), orthophosphoric acid (10.6 μL , 2.0 equiv.) dissolved in (0.5 mL) toluene was added dropwise. The reaction mixture was stirred at 50 $^\circ\text{C}$ for 5 h under N_2 atmosphere until its completion. Next, the reaction was quenched via water, extracted with EtOAc and the combined organic extracts dried over Na_2SO_4 , and evaporated *in vacuo*. The crude mixture was purified on silica column chromatography (eluent: *n*-hexane/DCM/ethyl acetate = 7/1/1) to give double 3-Hydroxy benzo[c]carbazole **2** as a white solid in 54% yield.

- 7,7'-(1,4-Phenylene)bis(7H-benzo[c]carbazol-10-ol) **2**

^1H NMR (600 MHz, $(\text{CD}_3)_2\text{CO}$): δ 8.80 (d, $J = 8.2$ Hz, 2H), 8.31 (s, 2H), 8.17 (d, $J = 2.1$ Hz, 2H), 8.07 (d, $J = 8.2$ Hz, 2H), 7.92–7.96 (m, 6H), 7.75–7.78 (m, 4H), 7.58 (d, $J = 8.9$ Hz, 2H), 7.50 (dd, $J = 8.3, 6.9$ Hz, 2H), 7.14 (dd, $J = 8.6, 2.4$ Hz, 2H); ^{13}C NMR (151 MHz, $(\text{CD}_3)_2\text{CO}$): δ 153.39, 139.70, 137.52, 135.41, 130.82, 130.43, 130.13, 129.80, 128.33, 127.95, 125.47, 123.91, 123.75, 115.93, 115.05, 112.67, 111.86, 107.78; DEPT-135 NMR (151 MHz, $(\text{CD}_3)_2\text{CO}$): δ 130.12, 129.80, 128.32, 127.95, 123.91, 123.74, 115.03, 112.67, 111.86, 107.76; HRMS (APCI): calcd for

$C_{38}H_{24}N_2O_2$: m/z 541.1911 $[M + H]^+$, found 541.1912.; IR (KBr): 3334, 3042, 2977, 2926, 1620, 1517, 1473, 1165, 831, 803 cm^{-1} ; mp: 198–199 °C.

3.2.2. General Procedure for the Synthesis of Double Aza-oxa[7]helicene 3

A 10 mL DCM solution of **2** (54 mg, 0.1 mmol), β -naphthol (57.7 mg, 0.4 mmol), tetrabutylammonium hexafluorophosphate(V) (387.4 mg, 1.0 mmol), and BF_3OEt_2 (0.2 M) was transferred into the undivided electrolysis cell of ElectraSyn[®] 2.0. This cell is equipped with two Pt electrodes connected to a DC power supply. At room temperature, a constant current of 1.5 mA was applied for 3.5 h. After the completion of reaction, the electrolysis was stopped and crude mixture was purified by column chromatography (SiO_2 , EtOAc/*n*-hexane) to afford the double aza-oxa[7]helicene **3** as a yellow solid in 26% yield.

• 1,4-Bis(10*H*-benzo[*c*]naphtho[1',2':4,5]furo[3,2-*g*]carbazol-10-yl)benzene **3**

1H NMR (600 MHz, $CDCl_3$): δ 8.38 (d, $J = 8.2$ Hz, 2H), 8.31 (d, $J = 8.2$ Hz, 2H), 8.00–8.04 (m, 12H), 7.92 (d, $J = 8.9$ Hz, 2H), 7.85 (d, $J = 8.9$ Hz, 4H), 7.77 (d, $J = 8.9$ Hz, 2H), 7.34–7.39 (m, 4H), 6.95–7.00 (m, 4H); ^{13}C NMR (151 MHz, $CDCl_3$): δ 154.75, 153.31, 138.79, 137.93, 137.32, 130.86, 129.79, 129.73, 129.50, 129.15, 128.59, 128.10, 128.05, 128.03, 125.13, 124.67, 124.37, 123.62, 120.07, 117.98, 117.77, 116.64, 112.65, 111.58, 109.45, 109.06 (Two carbons overlapped); DEPT-135 NMR (151 MHz, $CDCl_3$): δ 129.79, 129.15, 128.59, 128.09, 128.05, 128.03, 125.13, 124.67, 124.37, 123.61, 112.66, 111.58, 109.44, 109.06 (One carbon overlapped); HRMS (APCI): calcd for $C_{58}H_{32}N_2O_2$: m/z 789.2537 $[M + H]^+$, found 789.2542; IR (KBr): 3043, 2926, 2856, 1714, 1594, 1500, 1417, 1355, 1209, 805 cm^{-1} ; mp: 291–292 °C.

3.3. DFT Calculations

All DFT calculations were performed using the Gaussian 16 package of programs [63]. The geometries of the model compounds were optimized using three DFT functions: B3LYP, wB97XD, and MN15 at 6-311G(d,p) basis set. All stationary points were identified as stable minima by frequency calculations. Geometry optimization was achieved using the normal criteria defined in Gaussian 16. TD-DFT calculations were performed using two different levels of theory B3LYP/6-311G(d,p) and MN15/6-311G(d,p) in both chloroform and gas-phase. All structures were optimized without any symmetry assumptions. For further computational details, see Supplementary Materials.

4. Conclusions

In summary, we introduced a two-step protocol to synthesize double aza-oxa[7]helicene **3** using an electrochemical approach. This novel double hetero[7]helicene shows interesting structural features that were reflected in its excellent optical properties. We have studied the photophysical characteristics of this compound and correlated its absorption and fluorescence behavior based on DFT calculations. Further development for this two-step protocol towards the preparation of other multiple helicenes and PHAs and study their photophysical and chiroptical features are currently under investigation.

Supplementary Materials: The following supporting information can be downloaded at: <https://www.mdpi.com/article/10.3390/molecules27249068/s1>, Table S1: Optimization of the acid-mediated annulation step; Table S2: Optimization of the electrochemical sequential reaction; Table S3: Selected experimental and calculated structural parameters of double aza-oxa[7]helicene **3**; Tables S4–S6: Summary of the TD-DFT calculation results of **3**; Scheme S1: A plausible mechanism for the electrochemical domino reaction; Figure S1: Crystal measurements; Figure S2: Measurements of the optimized structures; Figure S3: Selected molecular orbitals of **3**; Figure S4: Simulated UV-vis absorption and CD spectra of (*P,M*)-**3**; Figure S5: Further NICS(0) calculations [57,63–68].

Author Contributions: Conceptualization, supervision, and project administration, H.S. and S.T.; methodology, DFT calculations, investigation, data analysis, and writing original draft, M.S.H.S.; methodology, investigation, validation, and formal analysis A.S. and M.I.K. All authors have read and agreed to the published version of the manuscript.

Funding: This work was supported by JSPS KAKENHI Grant Numbers 22K06502 in Grant-in-Aid for Scientific Research (C), Transformative Research Areas (A) 21A204 Digitalization-driven Transformative Organic Synthesis (DigiTOS), 22KK0073 in Fund for the Promotion of Joint International Research (Fostering Joint International Research (B)) from the Ministry of Education, Culture, Sports, Science, and Technology (MEXT), and the Japan Society for the Promotion of Science (JSPS), JST CREST (No. JPMJCR20R1), and Hoansha Foundation.

Informed Consent Statement: The study does not involve humans.

Data Availability Statement: CIF of the crystal of **3** is available as Supplementary. The X-ray crystallographic coordinate for the structure reported in this study has been deposited at the Cambridge Crystallographic Data Centre (CCDC) under deposition numbers CCDC-2156335 (**3**). These data can be obtained free of charge from The Cambridge Crystallographic Data Centre via www.ccdc.cam.ac.uk/data_request/cif.

Acknowledgments: We thank Yoichi Hoshimoto for helping with chiral HPLC resolution. We acknowledge the technical staff of the Comprehensive Analysis Center of SANKEN.

Conflicts of Interest: The authors declare no conflict of interest.

Sample Availability: Samples of compound **3** are available from the corresponding author upon reasonable request.

References

1. Jakubec, M.; Storch, J. Recent advances in functionalizations of helicene backbone. *J. Org. Chem.* **2020**, *85*, 13415–13428. [[CrossRef](#)] [[PubMed](#)]
2. Gingras, M. One hundred years of helicene chemistry. Part 3: Applications and properties of carbohelicenes. *Chem. Soc. Rev.* **2013**, *42*, 1051–1095. [[CrossRef](#)] [[PubMed](#)]
3. Shen, Y.; Chen, C.-F. Helicenes: Synthesis and applications. *Chem. Rev.* **2012**, *112*, 1463–1535. [[CrossRef](#)] [[PubMed](#)]
4. Crassous, J.; Stara, I.G.; Stary, I. *Helicenes: Synthesis, Properties, and Applications*; John Wiley & Sons: Hoboken, NJ, USA, 2022.
5. Gingras, M. One hundred years of helicene chemistry. Part 1: Non-stereoselective syntheses of carbohelicenes. *Chem. Soc. Rev.* **2013**, *42*, 968–1006. [[CrossRef](#)]
6. Gingras, M.; Félix, G.; Peresutti, R. One hundred years of helicene chemistry. Part 2: Stereoselective syntheses and chiral separations of carbohelicenes. *Chem. Soc. Rev.* **2013**, *42*, 1007–1050. [[CrossRef](#)]
7. Yang, S.Y.; Qu, Y.K.; Liao, L.S.; Jiang, Z.Q.; Lee, S.T. Research progress of intramolecular π -stacked small molecules for device applications. *Adv. Mater.* **2022**, *34*, 2104125. [[CrossRef](#)]
8. Han, J.; Guo, S.; Lu, H.; Liu, S.; Zhao, Q.; Huang, W. Recent progress on circularly polarized luminescent materials for organic optoelectronic devices. *Adv. Opt. Mater.* **2018**, *6*, 1800538. [[CrossRef](#)]
9. Jeon, S.K.; Lee, H.L.; Yook, K.S.; Lee, J.Y. Recent progress of the lifetime of organic light-emitting diodes based on thermally activated delayed fluorescent material. *Adv. Mater.* **2019**, *31*, 1803524. [[CrossRef](#)]
10. Zhang, C.; Wang, X.; Qiu, L. Circularly polarized photodetectors based on chiral materials: A review. *Front. Chem.* **2021**, *9*, 711488. [[CrossRef](#)]
11. Brandt, J.R.; Salerno, F.; Fuchter, M.J. The added value of small-molecule chirality in technological applications. *Nat. Rev. Chem.* **2017**, *1*, 0045. [[CrossRef](#)]
12. Shang, X.; Wan, L.; Wang, L.; Gao, F.; Li, H. Emerging materials for circularly polarized light detection. *J. Mater. Chem. C* **2022**, *10*, 2400–2410. [[CrossRef](#)]
13. Li, Q.; Zhang, Y.; Xie, Z.; Zhen, Y.; Hu, W.; Dong, H. Polycyclic aromatic hydrocarbon-based organic semiconductors: Ring-closing synthesis and optoelectronic properties. *J. Mater. Chem. C* **2022**, *10*, 2411–2430. [[CrossRef](#)]
14. Hong, J.; Xiao, X.; Liu, H.; Dmitrieva, E.; Popov, A.A.; Yu, Z.; Li, M.D.; Ohto, T.; Liu, J.; Narita, A.; et al. Controlling the emissive, chiroptical, and electrochemical properties of double [7]helicenes through embedded aromatic rings. *Chem. Eur. J.* **2022**, *28*, e202202243. [[CrossRef](#)] [[PubMed](#)]
15. Tian, Y.-H.; Park, G.; Kertesz, M. Electronic structure of helicenes, C₂S helicenes, and thiaheterohelicenes. *Chem. Mater.* **2008**, *20*, 3266–3277. [[CrossRef](#)]
16. Rajca, A.; Wang, H.; Pink, M.; Rajca, S. Annelated heptathiophene: A fragment of a carbon–sulfur helix. *Angew. Chem. Int. Ed.* **2000**, *39*, 4481–4483. [[CrossRef](#)]
17. Pieters, G.; Gaucher, A.; Marque, S.; Maurel, F.o.; Lesot, P.; Prim, D. Regio-defined amino [5]oxa- and thiahelicenes: A dramatic impact of the nature of the heteroatom on the helical shape and racemization barriers. *J. Org. Chem.* **2010**, *75*, 2096–2098. [[CrossRef](#)]
18. Nakano, K.; Oyama, H.; Nishimura, Y.; Nakasako, S.; Nozaki, K. λ^5 -Phospha[7]helicenes: Synthesis, properties, and columnar aggregation with one-way chirality. *Angew. Chem. Int. Ed.* **2012**, *51*, 695–699. [[CrossRef](#)]

19. Žádný, J.; Jančařík, A.; Andronova, A.; Šámal, M.; Vacek Chocholoušová, J.; Vacek, J.; Pohl, R.; Šaman, D.; Císařová, I.; Stará, I.G.; et al. A general approach to optically pure [5]-, [6]-, and [7]heterohelicenes. *Angew. Chem. Int. Ed.* **2012**, *51*, 5857–5861. [[CrossRef](#)]
20. Sundar, M.S.; Bedekar, A.V. Synthesis and study of 7,12,17-trioxa[11]helicene. *Org. Lett.* **2015**, *17*, 5808–5811. [[CrossRef](#)]
21. Schickedanz, K.; Trageser, T.; Bolte, M.; Lerner, H.-W.; Wagner, M. A boron-doped helicene as a highly soluble, benchtop-stable green emitter. *Chem. Commun.* **2015**, *51*, 15808–15810. [[CrossRef](#)]
22. Mori, T. Chiroptical properties of symmetric double, triple, and multiple helicenes. *Chem. Rev.* **2021**, *121*, 2373–2412. [[CrossRef](#)] [[PubMed](#)]
23. Tsurusaki, A.; Kamikawa, K. Multiple helicenes featuring synthetic approaches and molecular structures. *Chem. Lett.* **2021**, *50*, 1913–1932. [[CrossRef](#)]
24. Li, C.; Yang, Y.; Miao, Q. Recent progress in chemistry of multiple helicenes. *Chem. Asian J.* **2018**, *13*, 884–894. [[CrossRef](#)]
25. Shen, C.; Gan, F.; Zhang, G.; Ding, Y.; Wang, J.; Wang, R.; Crassous, J.; Qiu, H. Helicene-derived aggregation-induced emission conjugates with highly tunable circularly polarized luminescence. *Mater. Chem. Front.* **2020**, *4*, 837–844. [[CrossRef](#)]
26. Meng, D.; Fu, H.; Xiao, C.; Meng, X.; Winands, T.; Ma, W.; Wei, W.; Fan, B.; Huo, L.; Doltsinis, N.L.; et al. Three-bladed rylene propellers with three-dimensional network assembly for organic electronics. *J. Am. Chem. Soc.* **2016**, *138*, 10184–10190. [[CrossRef](#)] [[PubMed](#)]
27. Meng, D.; Liu, G.; Xiao, C.; Shi, Y.; Zhang, L.; Jiang, L.; Baldrige, K.K.; Li, Y.; Siegel, J.S.; Wang, Z. Corannulylene pentapetales. *J. Am. Chem. Soc.* **2019**, *141*, 5402–5408. [[CrossRef](#)] [[PubMed](#)]
28. Lin, Y.-C.; Chen, C.-H.; She, N.-Z.; Juan, C.-Y.; Chang, B.; Li, M.-H.; Wang, H.-C.; Cheng, H.-W.; Yabushita, A.; Yang, Y.; et al. Twisted-graphene-like perylene diimide with dangling functional chromophores as tunable small-molecule acceptors in binary-blend active layers of organic photovoltaics. *J. Mater. Chem. A* **2021**, *9*, 20510–20517. [[CrossRef](#)]
29. Lin, Y.-C.; She, N.-Z.; Chen, C.-H.; Yabushita, A.; Lin, H.; Li, M.-H.; Chang, B.; Hsueh, T.-F.; Tsai, B.-S.; Chen, P.-T.; et al. Perylene diimide-fused dithiophenepyrroles with different end groups as acceptors for organic photovoltaics. *ACS Appl. Mater. Interfaces* **2022**, *14*, 37990–38003. [[CrossRef](#)]
30. Yang, W.W.; Shen, J.J. Multiple heterohelicenes: Synthesis, properties and applications. *Chem. Eur. J.* **2022**, *28*, e202202069. [[CrossRef](#)]
31. Shiraiishi, K.; Rajca, A.; Pink, M.; Rajca, S. π -Conjugated conjoined double helicene via a sequence of three oxidative CC- and NN-homocouplings. *J. Am. Chem. Soc.* **2005**, *127*, 9312–9313. [[CrossRef](#)]
32. Wang, Z.; Shi, J.; Wang, J.; Li, C.; Tian, X.; Cheng, Y.; Wang, H. Syntheses and crystal structures of benzo[6]helicene and naphthalene cored double helicene. *Org. Lett.* **2010**, *12*, 456–459. [[CrossRef](#)] [[PubMed](#)]
33. Hashimoto, S.; Nakatsuka, S.; Nakamura, M.; Hatakeyama, T. Construction of a highly distorted benzene ring in a double helicene. *Angew. Chem. Int. Ed.* **2014**, *53*, 14074–14076. [[CrossRef](#)] [[PubMed](#)]
34. Nakamura, K.; Furumi, S.; Takeuchi, M.; Shibuya, T.; Tanaka, K. Enantioselective synthesis and enhanced circularly polarized luminescence of S-shaped double azahelicenes. *J. Am. Chem. Soc.* **2014**, *136*, 5555–5558. [[CrossRef](#)] [[PubMed](#)]
35. Chang, H.; Liu, H.; Dmitrieva, E.; Chen, Q.; Ma, J.; He, P.; Liu, P.; Popov, A.A.; Cao, X.-Y.; Wang, X.-Y.; et al. Furan-containing double tetraoxa[7]helicene and its radical cation. *Chem. Commun.* **2020**, *56*, 15181–15184. [[CrossRef](#)]
36. Terada, N.; Uematsu, K.; Higuchi, R.; Tokimaru, Y.; Sato, Y.; Nakano, K.; Nozaki, K. Synthesis and properties of spiro-double sila[7]helicene: The LUMO spiro-conjugation. *Chem. Eur. J.* **2021**, *27*, 9342–9349. [[CrossRef](#)]
37. Zhang, L.; Song, I.; Ahn, J.; Han, M.; Linares, M.; Surin, M.; Zhang, H.-J.; Oh, J.H.; Lin, J. π -Extended perylene diimide double-heterohelicenes as ambipolar organic semiconductors for broadband circularly polarized light detection. *Nat. Commun.* **2021**, *12*, 142. [[CrossRef](#)]
38. Fujikawa, T.; Mitoma, N.; Wakamiya, A.; Saeki, A.; Segawa, Y.; Itami, K. Synthesis, properties, and crystal structures of π -extended double [6]helicenes: Contorted multi-dimensional stacking lattice. *Org. Biomol. Chem.* **2017**, *15*, 4697–4703. [[CrossRef](#)]
39. Sun, Z.; Yi, C.; Liang, Q.; Bingi, C.; Zhu, W.; Qiang, P.; Wu, D.; Zhang, F. π -Extended C_2 -symmetric double NBN-heterohelicenes with exceptional luminescent properties. *Org. Lett.* **2019**, *22*, 209–213. [[CrossRef](#)]
40. Liu, X.; Yu, P.; Xu, L.; Yang, J.; Shi, J.; Wang, Z.; Cheng, Y.; Wang, H. Synthesis for the mesomer and racemate of thiophene-based double helicene under irradiation. *J. Org. Chem.* **2013**, *78*, 6316–6321. [[CrossRef](#)]
41. Sakamaki, D.; Kumano, D.; Yashima, E.; Seki, S. A facile and versatile approach to double N-heterohelicenes: Tandem oxidative C-N couplings of N-heteroacenes via cruciform dimers. *Angew. Chem. Int. Ed.* **2015**, *54*, 5404–5407. [[CrossRef](#)]
42. Katayama, T.; Nakatsuka, S.; Hirai, H.; Yasuda, N.; Kumar, J.; Kawai, T.; Hatakeyama, T. Two-step synthesis of boron-fused double helicenes. *J. Am. Chem. Soc.* **2016**, *138*, 5210–5213. [[CrossRef](#)] [[PubMed](#)]
43. Sakamaki, D.; Tanaka, S.; Tanaka, K.; Takino, M.; Gon, M.; Tanaka, K.; Hirose, T.; Hirobe, D.; Yamamoto, H.M.; Fujiwara, H. Double heterohelicenes composed of benzo [b]- and dibenzo [b, i] phenoxazine: A comprehensive comparison of their electronic and chiroptical properties. *J. Phys. Chem. Lett.* **2021**, *12*, 9283–9292. [[CrossRef](#)] [[PubMed](#)]
44. Wang, X.-Y.; Wang, X.-C.; Narita, A.; Wagner, M.; Cao, X.-Y.; Feng, X.; Müllen, K. Synthesis, structure, and chiroptical properties of a double [7]heterohelicene. *J. Am. Chem. Soc.* **2016**, *138*, 12783–12786. [[CrossRef](#)] [[PubMed](#)]
45. Li, J.-K.; Chen, X.-Y.; Guo, Y.-L.; Wang, X.-C.; Sue, A.C.-H.; Cao, X.-Y.; Wang, X.-Y. B,N-embedded double hetero[7]helicenes with strong chiroptical responses in the visible light region. *J. Am. Chem. Soc.* **2021**, *143*, 17958–17963. [[CrossRef](#)]

46. Salem, M.S.H.; Khalid, M.I.; Sako, M.; Higashida, K.; Lacroix, C.; Kondo, M.; Takishima, R.; Taniguchi, T.; Miura, M.; Vo-Thanh, G.; et al. Electrochemical synthesis of aza-oxa[7]helicenes via an oxidative heterocoupling and dehydrative cyclization sequence. *Molecules*, 2022; Submitted.
47. Khalid, M.I.; Salem, M.S.H.; Sako, M.; Kondo, M.; Sasai, H.; Takizawa, S. Electrochemical synthesis of heterodehydro[7]helicenes. *Commun. Chem.* **2022**, *5*, 166. [[CrossRef](#)]
48. Pushkarskaya, E.; Wong, B.; Han, C.; Capomolla, S.; Gu, C.; Stoltz, B.M.; Zhang, H. Single-step synthesis of 3-hydroxycarbazoles by annulation of electron-rich anilines and quinones. *Tetrahedron Lett.* **2016**, *57*, 5653–5657. [[CrossRef](#)]
49. Mei, J.; Diao, Y.; Appleton, A.L.; Fang, L.; Bao, Z. Integrated materials design of organic semiconductors for field-effect transistors. *J. Am. Chem. Soc.* **2013**, *135*, 6724–6746. [[CrossRef](#)]
50. Rivnay, J.; Jimison, L.H.; Northrup, J.E.; Toney, M.F.; Noriega, R.; Lu, S.; Marks, T.J.; Facchetti, A.; Salleo, A. Large modulation of carrier transport by grain-boundary molecular packing and microstructure in organic thin films. *Nat. Mater.* **2009**, *8*, 952–958. [[CrossRef](#)]
51. Minemawari, H.; Tanaka, M.; Tsuzuki, S.; Inoue, S.; Yamada, T.; Kumai, R.; Shimoi, Y.; Hasegawa, T. Enhanced layered-herringbone packing due to long alkyl chain substitution in solution-processable organic semiconductors. *Chem. Mater.* **2017**, *29*, 1245–1254. [[CrossRef](#)]
52. Sun, Q.; Ren, J.; Jiang, T.; Peng, Q.; Ou, Q.; Shuai, Z. Intermolecular charge-transfer-induced strong optical emission from herringbone H-Aggregates. *Nano Lett.* **2021**, *21*, 5394–5400. [[CrossRef](#)]
53. Gierschner, J.; Ehni, M.; Egelhaaf, H.-J.; Milián Medina, B.; Beljonne, D.; Benmansour, H.; Bazan, G.C. Solid-state optical properties of linear polyconjugated molecules: π -stack contra herringbone. *J. Chem. Phys.* **2005**, *123*, 144914–144922. [[CrossRef](#)] [[PubMed](#)]
54. Kirstein, S.; Möhwald, H. Herringbone structure in two-dimensional single crystals of cyanine dyes. II. Optical properties. *J. Chem. Phys.* **1995**, *103*, 826–833. [[CrossRef](#)]
55. Furche, F.; Ahlrichs, R.; Wachsmann, C.; Weber, E.; Sobanski, A.; Vögtle, F.; Grimme, S. Circular dichroism of helicenes investigated by time-dependent density functional theory. *J. Am. Chem. Soc.* **2000**, *122*, 1717–1724. [[CrossRef](#)]
56. Demissie, T.B.; Sundar, M.S.; Thangavel, K.; Andrushchenko, V.; Bedekar, A.V.; Bouř, P. Origins of optical activity in an oxo-helicene: Experimental and computational studies. *ACS Omega* **2021**, *6*, 2420–2428. [[CrossRef](#)] [[PubMed](#)]
57. Haoyu, S.Y.; He, X.; Li, S.L.; Truhlar, D.G. MN15: A Kohn–Sham global-hybrid exchange–correlation density functional with broad accuracy for multi-reference and single-reference systems and noncovalent interactions. *Chem. Sci.* **2016**, *7*, 5032–5051.
58. Lin, H.A.; Sato, Y.; Segawa, Y.; Nishihara, T.; Sugimoto, N.; Scott, L.T.; Higashiyama, T.; Itami, K. A water-soluble warped nanographene: Synthesis and applications for photoinduced cell death. *Angew. Chem. Int. Ed.* **2018**, *57*, 2874–2878. [[CrossRef](#)]
59. Liu, C.; Zhang, S.; Li, J.; Wei, J.; Müllen, K.; Yin, M. A water-soluble, NIR-absorbing quaterrylenediimide chromophore for photoacoustic imaging and efficient photothermal cancer therapy. *Angew. Chem. Int. Ed.* **2019**, *58*, 1638–1642. [[CrossRef](#)]
60. Matsuo, Y.; Chen, F.; Kise, K.; Tanaka, T.; Osuka, A. Facile synthesis of fluorescent hetero[8]circulene analogues with tunable solubilities and optical properties. *Chem. Sci.* **2019**, *10*, 11006–11012. [[CrossRef](#)]
61. Bredas, J.L.; Silbey, R.; Boudreaux, D.S.; Chance, R.R. Chain-length dependence of electronic and electrochemical properties of conjugated systems: Polyacetylene, polyphenylene, polythiophene, and polypyrrole. *J. Am. Chem. Soc.* **1983**, *105*, 6555–6559. [[CrossRef](#)]
62. Yan, M.; Kawamata, Y.; Baran, P.S. Synthetic organic electrochemistry: Calling all engineers. *Angew. Chem. Int. Ed.* **2018**, *57*, 4149–4155. [[CrossRef](#)]
63. Frisch, M.E.; Trucks, G.; Schlegel, H.; Scuseria, G.; Robb, M.; Cheeseman, J.; Scalmani, G.; Barone, V.; Petersson, G.; Nakatsuji, H. *Gaussian 16, Rev. C.01*; Gaussian Inc.: Wallingford, CT, USA, 2016.
64. Casida, M.E.; Jamorski, C.; Casida, K.C.; Salahub, D.R. Molecular excitation energies to high-lying bound states from time-dependent density-functional response theory: Characterization and correction of the time-dependent local density approximation ionization threshold. *J. Chem. Phys.* **1998**, *108*, 4439–4449. [[CrossRef](#)]
65. Stratmann, R.E.; Scuseria, G.E.; Frisch, M.J. An efficient implementation of time-dependent density-functional theory for the calculation of excitation energies of large molecules. *J. Chem. Phys.* **1998**, *109*, 8218–8224. [[CrossRef](#)]
66. Wolinski, K.; Hinton, J.F.; Pulay, P. Efficient implementation of the gauge-independent atomic orbital method for NMR chemical shift calculations. *J. Am. Chem. Soc.* **1990**, *112*, 8251–8260. [[CrossRef](#)]
67. Bühl, M.; van Wüllen, C. Computational evidence for a new C84 isomer. *Chem. Phys. Lett.* **1995**, *247*, 63–68. [[CrossRef](#)]
68. Schleyer, P.V.R.; Maerker, C.; Dransfeld, A.; Jiao, H.; van Eikema Hommes, N.J. Nucleus-independent chemical shifts: A simple and efficient aromaticity probe. *J. Am. Chem. Soc.* **1996**, *118*, 6317–6318. [[CrossRef](#)]